Synthesis, Derivatization, and Structural Analysis of Phosphorylated Mono-, Di-, and Trifluorinated D-Gluco-heptuloses by Glucokinase: Tunable Phosphoglucomutase Inhibition

Jian-She Zhu,[†] Kyle M. Stiers,[‡] Sherany M. Winter,[†,§,¶] Anthony D. Garcia,[†,∥,¶] Antoine F. Versini,[†,⊥,¶] Lesa J. Beamer,*,[†] and David L. Jakeman*,[†,#]

[†]College of Pharmacy, Dalhousie University, 5968 College Street, Halifax, Nova Scotia B3H 4R2, Canada
[‡]Biochemistry Department, University of Missouri, 117 Schweitzer Hall, Columbia, Missouri 65211, United States
[§]Department of Chemistry, Hogeschool Leiden (UAS Leiden), Zernikedreef 11, CK Leiden 2333, The Netherlands
[∥]École Nationale Supérieure de Chimie de Rennes, 11 Allée de Beaulieu, CS 50837, Rennes Cedex 7 35708, France
[⊥]École Supérieure de Physique et de Chimie Industrielles de la Ville de Paris, 10 rue Vauquelin, Paris 75005, France
[#]Department of Chemistry, Dalhousie University, Halifax, Nova Scotia B3H 4R2, Canada

S Supporting Information
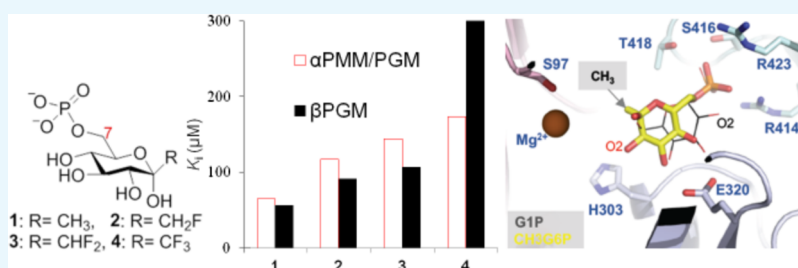
ABSTRACT: Glucokinase phosphorylated a series of C-1 fluorinated α-D-gluco-heptuloses. These phosphorylated products were discovered to be inhibitors of α-phosphomannomutase/phosphoglucomutase (αPMM/PGM) and β-phosphoglucomutase (βPGM). Inhibition potency with both mutases inversely correlated to the degree of fluorination. Structural analysis with αPMM demonstrated the inhibitor binding to the active site, with the phosphate in the phosphate binding site and the anomeric hydroxyl directed to the catalytic site.

INTRODUCTION

Ketoheptoses are rare naturally occurring seven-membered sugars that are receiving increasing attention due to their potential pharmaceutical applications in the treatment of hypoglycemia or cancer.[1] Ketoheptoses, especially D-manno-heptulose (Figure 1), as a substrate for noninvasive imaging of
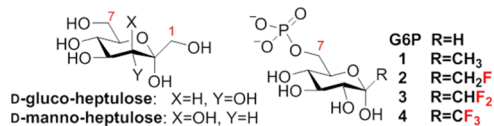

Figure 1. Representative ketoheptoses and C-1 fluorinated α-D-glucoheptulose 7-phosphates1-4 prepared herein.

β-cells,[1] provides an alternative tool in diabetes diagnosis or therapies that depend on β-cell mass visualization and quantitative analysis.[2] Recently, it was found that fluorinated heptulose analogues functioned as tools for the noninvasive imaging of GLUT2-expressing insulin-producing cells by ^{19}F magnetic resonance imaging ([19]FMRI).[3] In order to evaluate their spectrum of potential biological activities, ketoheptose

analogues have been accessed by either chemical[1,4] or enzymatic[5] methods, with fluorinated carbohydrates as prominent tools to study various biochemical processes including structural and mechanistic investigations,[6] radio-labeling,[7] lectin−carbohydrate interactions,[8] and carbohydrate lipophilicity.[9] Further functionalization of ketoheptoses will provide access to mechanistic probes such as C-glycosides or analogues of glucose 6-phosphate (G6P) or glucose 1-phosphate (G1P). However, to date, such phosphorylated fluorinated ketoheptoses have not been prepared or evaluated. Synthetic access would provide opportunities to explore a variety of biological systems, including probing the structure and function of phosphoglucomutases (PGMs).

PGMs catalyze the reversible intramolecular conversion of G6P to G1P, and play essential biological roles in numerous living organisms from bacteria to humans.[10] There are two different classes of PGMs, α-phosphoglucomutases (αPGM) and β-phosphoglucomutase (βPGM), differing in the substrate

anomer and enzyme mechanism of action. βPGM from *Lactococcus lactis* (*L. lactis*), a member of haloacid dehalogenase superfamily,[11] is essential in the maltose and trehalose catabolic pathway of *L. lactis*.[12] α-Phosphomannomutase/PGM (αPMM/PGM) from *Pseudomonas aeruginosa* (*P. aeruginosa*) belongs to the α-D-phosphohexomutases family and has dual substrate specificity for α-mannose 1-phosphate and αG1P.[13] In *P. aeruginosa*, αPMM/PGM is involved in the biosynthesis of alginate, B-band lipopolysaccharide (LPS), rhamnolipid, and the LPS-core.[14] These polysaccharides are essential components of the bacterial cell wall and are implicated in *P. aeruginosa* virulence. Additionally, *P. aeruginosa* is a deadly opportunistic human pathogen listed as a significant threat by the World Health Organization.[15] These data make this enzyme a potential target for antibacterial drug design.

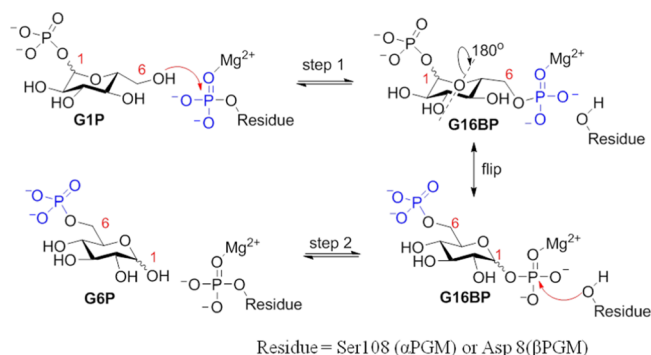Both enzymes share a similar mechanistic pathway, consisting of two enzymatic phosphorylations (Figure 2),[13]

Figure 2. Reactions catalyzed by α- and β-PGM.

involving a single active site phosphoenzyme, which is serine (Ser) in αPGM and aspartic acid (Asp) in βPGM. The first step involves the transfer of the phosphoryl group from the phosphoenzyme to the C6−OH group of G1P, and formation of an intermediate glucose 1,6-bisphosphate (G16BP). After reorientation and rebinding to the active site, this intermediate (step 2) is converted to product G6P by phosphoryl transfer back to the dephosphoenzyme from the C1−OH group, thus finishing the catalytic cycle.

Early probes into the mechanism of αPGM include galactose 1,6-bisphosphate[16] and fructose 2,6-bisphosphate,[17] as G16BP analogues, whereas 1-deoxyglucose 6-phosphate was evaluated as an inhibitor of αPMM/PGM from *P. aeruginosa*.[18] Attempts to inhibit αPGM covalently have included evaluation of sugar phosphofluoridates, sugar cyclic phosphates,[19] and nojirimycin 6-phosphate.[20] Metal complexes have also been studied, as mimics of the transferred phosphate, including with αPGM and 6-vanadate-αG1P[21] and more recently with βPGM in aluminum and magnesium fluoride complexes,[22] together with the G6P[23] and with the nonhydrolyzable monofluoromethylene phosphonate substrate analogues that enabled access to the first βPGM phosphoryl transfer step.[24]

Herein, we describe *Escherichia coli* glucokinase (Glk)-catalyzed phosphorylation of a series of C-1 fluorinated α-D-gluco-heptuloses, and evaluation of the 7-phosphates **1−4**, as αG6P analogues, against both α- and β-phosphoglucomutases.

■ RESULTS AND DISCUSSION

It was envisioned that the αG6P analogues, **1−4** could be accessible by an *E. coli* Glk[25]-catalyzed phosphorylation of the 7-OH group of the appropriate C-1 fluorinated ketoses, in turn obtained from global debenzylation of compounds, **8−11** (Scheme 1). These intermediates were all readily obtained

Scheme 1. Synthesis of (a) compound 8 and (b) 1−4
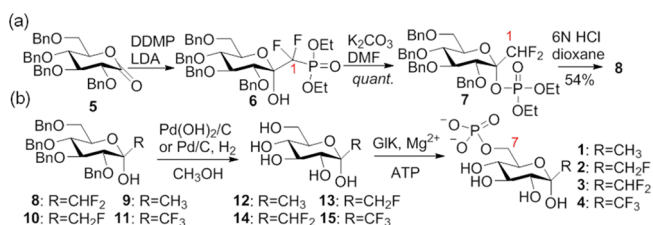
starting from protected gluconolactone **5**. Methylated compound **9**,[26] monofluoromethylated compound **10**,[27] and trifluoromethylated compound **11**[28] were readily prepared, starting from **5** according to the reported procedures, where nucleophilic addition of commercially available CH₃Li and TMSCF₃ to **5** furnished **9** and **11**, respectively. In contrast, the direct synthesis of the difluoromethylated compound **8** required a different approach due to lack of a convenient difluoromethyl nucleophile. As a result, diethyl difluoromethyl phosphonate (DDMP)[29] was utilized for this purpose.

The synthesis of compound **8** (Scheme 1a) commenced with **6**, prepared by nucleophilic addition of DDMP to **5**.[30] The resultant phosphonate **6** then rearranged at 55 °C with anhydrous K₂CO₃ to yield phosphate **7** quantitatively. The rearranged structure **7** was confirmed by analysis of NMR data. In the ¹H NMR spectrum of **7**, a new triplet signal at 6.6 ppm was assigned as H-1. Additionally, a doublet of signals for each fluorine and a singlet signal were observed in the ¹⁹F{¹H} and ³¹P{¹H} NMR spectra of **7**, respectively (Figure S1 in the Supporting Information). By comparison for **6**, the fluorine and phosphorus signals were an ABX spin system and a triplet in the ¹⁹F{¹H} and ³¹P{¹H} NMR, respectively, arising from ¹⁹F−¹⁹F and ¹⁹F−³¹P coupling (Figure S1 in the Supporting Information). Finally, acidic hydrolysis of the phosphate group in **7** with 6 N HCl/1,4-dioxane afforded **8** in 54% yield, with spectroscopic data consistent with those reported.[31] This method to make **8** is very efficient, on the gram scale with 40% overall yield from **5** with column chromatography only after the final step. This is the first time this rearrangement incorporates a difluoromethyl group into a carbohydrate.

Compounds **8−11** were subjected to hydrogenolysis (Scheme 1b) with either Pd(OH)₂/C−H₂ or Pd/C−H₂ to provide the corresponding α-D-gluco-heptulose analogues, **12−15** in quantitative yields. Compound **13** is known to inhibit glucose metabolism and insulin secretion and also has potential as a tracer for the noninvasive imaging of hepatocytes and insulin producing cells by ¹⁹FMRI.[3] Therefore, the difluoro and trifluoro compounds **14** and **15** may have similar utility.

Glk is known as a glucokinase rather than a hexokinase, which specifically phosphorylates gluco-configured substrates.[25] Analogues **12−15** were examined as substrates of Glk, utilizing conditions described in the literature.[32] Recombinant Glk was found to efficiently convert all four C-1 fluoromethyl-modified G1P analogues (**12−15**) to corresponding 7-phosphorylated products. This result demonstrates that Glk tolerates a glucopyranose sugar modified at the anomeric center. Quantitative conversion of these compounds (Scheme 1b) on a milligram scale through overnight

incubation with Glk was achieved as observed by ^{1}H NMR or ^{19}F{^{1}H} NMR spectra. The pure products were then isolated exclusively as α-anomers in 73−98% yield by selective precipitation of adenosine diphosphate and adenosine triphosphate (ATP) with ethanol, followed by size exclusion chromatography.[32] The observation of a doublet signal for the C-7 ($^2J_{C-7,P}$ = 7.5 Hz) and C-6 ($^3J_{C-7,P}$ = 4.0 Hz) due to the ^{13}C−^{31}P coupling in the ^{13}C{^{1}H} NMR spectra of 1−4 further confirmed these G6P derivative structures.

Based on the anomeric configuration, it was hypothesized that these αG6P analogues could be potential substrates of αPMM/PGM from *P. aeruginosa* but inhibitors of βPGM from *L. lactis*. We were also curious about how these enzymes would respond to the increasingly bulkier and electronegative C-1 modification from 1 to 4. Initially compounds were evaluated as substrates. None of compounds 1−4 proved to be substrates of either αPMM/PGM from *P. aeruginosa* or βPGM from *L. lactis* up to a concentration of 0.2 mM, presumably due to the methyl substituent at C-1 blocking phosphoryl transfer by αPMM/PGM or βPGM (Scheme S1 in the Supporting Information). As a result, they were evaluated as potential inhibitors of these enzymes at various concentrations (0−1000 μM) by measuring their IC$_{50}$ values (Figure S3 and S4 in the Supporting Information) through a coupled assay, as described in the literature.[24b,33] It was noteworthy that these analogues (1−4), although structurally similar to G6P, showed no significant inhibition against G6P dehydrogenase, the second enzyme used in the coupled assay (a maximum of 15% inhibition at 5 mM inhibitor concentration was observed). The inhibition results of compounds 1−4 against αPMM/PGM and βPGM are summarized in Table 1.

Table 1. IC$_{50}$ Values of 1−4 against αPMM/PGM from *P. aeruginosa* and βPGM from *L. lactis*

compound	αPMM/PGM[a]		βPGM[b]	
	IC$_{50}$ (μM)	K_i (μM)[c]	IC$_{50}$ (μM)	K_i (μM)[c]
1	131 ± 1	65 ± 0.5	113 ± 3	57 ± 2
2	234 ± 29	117 ± 14	183 ± 14	92 ± 7
3	288 ± 37	144 ± 18	214 ± 11	107 ± 6
4	345 ± 55	174 ± 27	621 ± 82	310 ± 41

[a]K_m(αG1P) = 20 μM. [b]K_m(βG1P) = 9 μM.[24b] [c]Calculated from IC$_{50}$ data.[34]

The K_i values were calculated based on the IC$_{50}$ values, K_m, and substrate concentration using the published equations.[34] As the substrate concentration was equal to K_m under the assay conditions, K_i = 1/2IC$_{50}$ for either competitive or uncompetitive inhibitors, whereas K_i = IC$_{50}$ for the noncompetitive inhibitors. Based on the structural data (vide infra), the αG6P analogues (1−4) were assumed to be competitive inhibitors of αPMM/PGM from *P. aeruginosa* or βPGM from *L. lactis*, with K_i values calculated to be between 65 and 174 μM for αPMM/PGM and from 57 to 310 μM for βPGM. Interestingly, a trend was observed in that the IC$_{50}$ value increased in the order 1 to 4 against αPMM/PGM. This trend is in accordance with the increasing bulkiness[35] and electronegativity[36] of the substituent (CH$_3$ < CH$_2$F < CHF$_2$ < CF$_3$) at the anomeric center. It was noteworthy to find that this trend was also observed in the βPGM data, although these analogues are not in the enzyme-favored β-anomeric configuration. These results demonstrate that both αPMM/PGM and βPGM activity is tunable in

response to the steric component at the anomeric center of the physiological substrate, G6P.

To study the structural interactions of these G6P analogues with αPMM/PGM, we utilized the protein PGM from *Xanthomonas citri* (XcPGM),[13] a phytopathogen, known for being the causative agent of citrus canker. XcPGM is 34% identical overall in amino acid sequence to *P. aeruginosa* PMM/PGM, and active site residues in the two proteins are very highly conserved (Figure S5 in the Supporting Information). Crystals of XcPGM diffract to high resolution and are amenable to the formation of ligand complexes.[37] Crystal structures of XcPGM as apo-enzymes and in complexes with G1P and G16BP were previously published (PDB IDs: 5BMN, 5BMP, and 5KLO, respectively).[37] These structures are used for comparisons with 1:XcPGM below.

A high-resolution structure (1.7 Å) was obtained for XcPGM in complex with compound 1 (PDB ID: 6N1E). Successful complex formation is consistent with the K_i of this compound (Table 1). As seen in other ligand complexes of XcPGM,[37] binding of 1 produces a conformational change of the protein, relative to the apo-enzyme. This involves an active site loop in the C-terminal domain (cyan in Figure 3A) of the protein (residues 415−421) that closes around the inhibitor, essentially creating a lid over the active site. Thus, 1 is deeply buried in the active site cleft, with less than 20% of its surface area exposed to solvent.

It is convenient to consider the binding modes of compound 1 relative to the interactions of XcPGM with its substrate αG1P.[37] As first shown in crystallographic studies of αPMM/PGM,[38] binding of 1- and 6-phosphosugars involves similar enzyme contacts to the phosphate group of the ligand, while accommodating alternate orientations of the sugar ring in the active site. This arrangement is necessitated by the 180° flip of the G16BP intermediate, required by the enzyme mechanism (compare sugar ring orientation of αG1P and G6P in Figure 2). The XcPGM/1 complex provides characterization for a 6-phosphosugar complex. In particular, this includes interactions with Arg414, Arg423, Asn417, Ser416, and Thr418 of the phosphate (Figure 3B and Table S2), that is, the same residues used for phosphate binding in αG1P.

By contrast, interactions with the hydroxyls of the sugar ring vary significantly due to the alternate orientation of the sugar ring. Glu320 is able to maintain a key bidentate interaction with O3 and O4 because these hydroxyls essentially exchange places (Figure 3B). However, the backbone amide of His303 contacts O3 in the 1 complex, instead of O4 as in the G1P complex (Table S2). Other changes include loss of an interaction between Arg280 and O2 due to its distinct position in the 1 complex.[38] Overall, it appears that inhibitor 1 utilizes the expected binding interactions of a 6-phosphosugar with the enzyme, despite replacing the anomeric hydrogen atom with a methyl substituent. There are no protein atoms within 4.5 Å of this methyl group. Owing to the shared phosphate binding interactions with both G1P and 1, the observed binding mode is consistent with competitive inhibition (Table 1).

■ CONCLUSIONS

In conclusion, synthetic access to four C-1 fluorinated α-D-gluco-heptulose analogues was accomplished through chemical manipulations of gluconolactone 5. Derivatizing these heptulose analogues by *E. coli* Glk led to corresponding α-D-gluco-heptulose 7-phosphate analogues 1−4 that are inhibitors of both αPMM/PGM and βPGM. Inhibition potency against
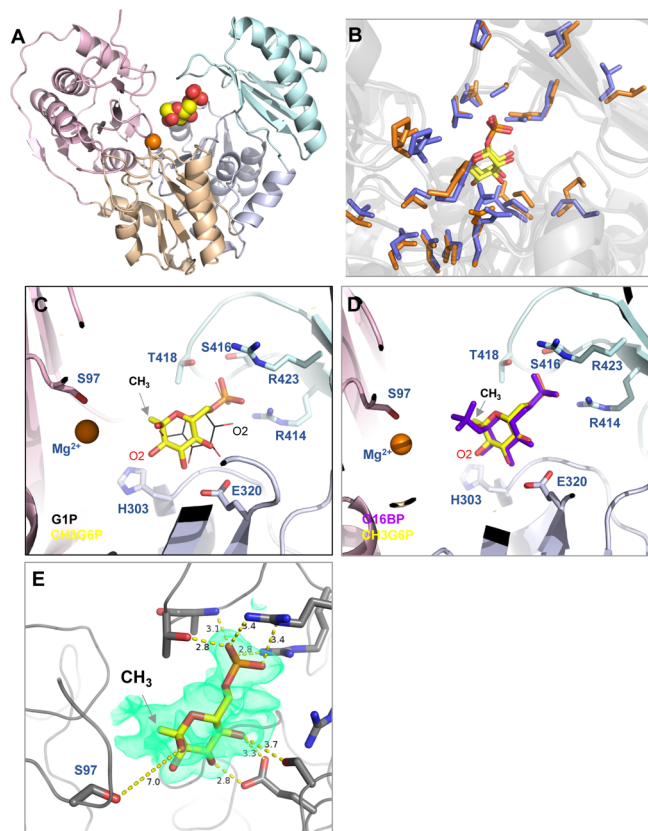
Figure 3. (A) Crystal structure of the XcPGM complex with inhibitor **1** (PDB 6N1E). Ligand is shown as a space-filling model; bound Mg^{2+} ion as an orange sphere. The protein is colored by domains as pink, beige, gray-blue, and cyan. (B) Structural superposition of *X. citri* αPGM (orange) and *P. aeruginosa* αPMM/PGM (blue), both in complex with substrate G1P (yellow). Side chains of identical residues are shown as sticks. Note the overall structural similarity of both polypeptide backbone and active-site side chains. (C) Close-up view of the active site showing a superposition of **1** (yellow) with G1P (black) from the substrate complex of XcPGM (PDB ID 5BMP). (D) Close-up view of the active site showing a superposition of **1** (yellow) with G16BP (purple) from the intermediate complex of XcPGM (PDB ID 5KL0). (E) Polder-style omit map showing the ligand-binding site in the enzyme-CH3G6P complex. Electron density (green) is contoured at 3.0 σ. Residues involved in interactions with ligands are shown as sticks. Hydrogen bond lengths and the distance from Ser97 to O1 of **1** are indicated.

both enzymes is dependent on the size and electronegativity of the substituted group at C-1 position, with the C-1 methylated G6P analogue (**1**), displaying the most significant inhibition. Both enzymes were found to be sensitive to the steric and electronic environment at the anomeric center of G6P. X-ray crystallographic analysis of **1** with XcPGM demonstrates that this inhibitor occupies the enzyme active site and that the methyl substituent does not form specific contacts with active-site residues. These structural insights will guide future potential antibacterial drug design targeting *P. aeruginosa* αPMM/PGM and will be reported in due course.

■ EXPERIMENTAL SECTION

General Methods and Instrumentation for Chemical Synthesis. All chemicals and reagents were purchased and used as received, unless noted otherwise. Anhydrous reaction conditions were maintained under an inert atmosphere of

dried high-purity nitrogen. Glassware was dried overnight in an oven at 120 °C and assembled under a stream of inert nitrogen. Thin layer chromatography plates were visualized by ultraviolet light at 254 and/or by charring after treatment with Vanillin stain. Flash chromatography was performed with silica gel 60 (230−400 mesh). Lyophilization of samples was carried out using a freeze-dryer. NMR spectra were recorded on a Bruker 300 or 500 MHz spectrometers. All ^{1}H, ^{13}C, ^{19}F, and ^{31}P chemical shifts are reported in ppm using tetramethylsilane (0.00 ppm) or the solvent signal [CDCl$_3$ (^{1}H 7.26 ppm; ^{13}C 77.16 ppm); D$_2$O (^{1}H 4.79 ppm)] as the internal reference or MeOD (^{13}C 49.50 ppm in D$_2$O) or 85% aq H$_3$PO$_4$ (^{31}P 0.00 ppm) as an external reference. Splitting patterns are indicated as follows: br, broad; s, singlet; d, doublet; t, triplet; at, apparent triplet; q, quartet; m, multiplet. All coupling constants (*J*) are reported in hertz (Hz). Mass spectra were recorded using ion trap (ESI TOF) instruments.

General Procedure: Glk-Catalyzed Synthesis of 7-Phospho Analogues. This followed the literature procedure with minor modifications.[32] A final volume of 4 mL (50 mM Tris−HCl, pH 7. 5) comprising 1-deoxy-α-D-glucoheptuloses (50 μM), MgCl$_2$ (102 mg, 500 μM), ATP (200 mM, 500 μL), and recombinant *E. coli* Glk (28 mg mL^{-1}, 110 μL) was incubated at 37 °C overnight.

The reaction mixture was quenched by the addition of three volumes of ethanol, followed by centrifugation at 5000*g* for 1 h at 4 °C. The supernatant was collected, and the solvent was evaporated in vacuo. The above manipulation was repeated once by re-dissolving the resultant material in millipore water (1 mL) and ethanol (9 mL). The resulting residue was then redissolved in 0.6 mL of distilled water and desalted by size exclusion chromatography (Sephadex LH20) eluting with millipore water. Fractions containing the product were collected, concentrated, and lyophilized.

1-Deoxy-α-D-gluco-heptulose 7-Phosphate (1). Lactone **5** was prepared from commercially available 2,3,4,6-tetra-*O*-benzyl glucopyranose, following a known procedure,[30] and then converted to **9** following a procedure described in the literature.[26] To a solution of compound **9** (100 mg, 0.18 mmol) in CH$_3$OH was added 20% wt Pd(OH)$_2$/C (30 mg). The suspension was degassed under vacuum and saturated with H$_2$ in a Parr Shaker at 60 psi pressure. This reaction mixture was shaken overnight. When the starting material disappeared completely, as determined by TLC monitoring, the catalyst was removed by filtration. The filtrate was concentrated under reduced pressure to give **12** (35 mg, 100%).

Data for Compound 9 (Figure S7). ^{1}H NMR (500 MHz, D$_2$O): δ 7.41−7.21 (m, 20H), 5.01−4.86 (m, 4H), 4.78−4.56 (m, 4H), 4.10−4.00 (m, 2H), 3.81−3.68 (m, 3H), 3.44−3.41 (m, 1H), 2.79 (s, br, 1H, OH), and 1.47 (s, 3H). This is consistent with the reported data.[39]

Data for Compound 12 (Figures S8 and S9). ^{1}H NMR (500 MHz, D$_2$O): δ 3.79 (dd, *J* = 11.5 and 2.0 Hz, 1H), 3.76−3.68 (m, 2H), 3.61 (t, *J* = 9.5 Hz, 1H), 3.35 (t, *J* = 9.5 Hz, 1H), and 3.24 (d, *J* = 9.5 Hz, 1H). ^{13}C NMR (125 MHz, D$_2$O): δ 97.5, 75.1, 73.6, 72.3, 69.9, 60.7, and 24.6. HRMS (ESI$^+$): found [M + Na]$^+$, 217.0692, C$_7$H$_{14}$NaO$_6$; requires [M + Na]$^+$, 217.0683.

Following the general procedure, **1** (18 mg, 86%) was obtained from compound **12** (15 mg, 31 μM), MgCl$_2$ (63 mg, 310 μM), ATP (200 mM, 310 μL), Glk (28 mg mL^{-1}, 72 μL), and Tris−HCl (50 mM, 3618 μL, pH 7.5).

Data for Compound 1 (Figures S10 and S12). ^{1}H NMR (500 MHz, D_2O): δ 4.05−3.95 (m, 2H), 3.85−3.83 (m, 1H), 3.63 (t, J = 5.0 Hz, 1H), 3.48 (t, J = 5.0 Hz, 1H), 3.28−3.26 (m, 1H), and 1.43 (s, 3H), ^{31}P{^{1}H} NMR (202 MHz, D_2O): δ 1.8. ^{13}C{^{1}H} NMR (125 MHz, D_2O): δ 97.7, 75.1, 73.4, 71.57 (d, $^2J_{C\text{-}7,P}$ = 7.5 Hz), 69.4, 63.7 (d, $^3J_{C\text{-}6,P}$ = 4.3 Hz), and 24.5. HRMS (ESI$^-$): found $[M − H]^-$, 273.0379, $C_7H_{14}O_9P$; requires $[M − H]^-$, 273.0381.

1-Deoxy-1-monofluoro-α-D-gluco-heptulose 7-Phosphate (2). Subject to a two-step transformation to generate compound **10** in 62% yield over two steps.[27] Data for **10** (Figure S13): ^{19}F NMR (470 MHz, DMSO-d_6): −226.2 (t, $^2J_{F,H}$ = 47.3 Hz). This is consistent with the reported data.[27]

To a solution of **10** (92 mg, 0.16 mmol) in CH_3OH was added 20% wt Pd(OH)$_2$/C (20 mg). The suspension was degassed under vacuum and saturated with H_2 under 1 atm pressure (balloon). This reaction mixture was stirred overnight. When the starting material disappeared completely, as determined by TLC monitoring, the catalyst was filtered off and the filtrate was concentrated under reduced pressure to give **13** (34 mg, 100%). Data for **13** (Figure S14): ^{19}F NMR (470 MHz, D_2O): −231.2 (t, $^2J_{F,H}$ = 47.3 Hz). This data is consistent with the reported data.[27]

Following the general procedure, **2** (10 mg, 73%) was obtained from compound **13** (10.0 mg, 47 μM), MgCl$_2$ (96 mg, 470 μM), ATP (200 mM, 472 μL), Glk (28 mg mL^{-1}, 110 μL), and Tris−HCl (50 mM, 3418 μL, pH 7.5).

Data for 2 (Figures S15−S18). ^{1}H NMR (500 MHz, D_2O): δ 4.50 (dd, $^2J_{H1a,F}$ = 45.0 Hz, $^2J_{H1a,H1b}$ = 10.0 Hz, 1H), 4.35 (dd, $^2J_{H1b,F}$ = 50.0 Hz, $^2J_{H1a,H1b}$ = 10.0 Hz, 1H), 4.03−3.99 (m, 1H), 3.93 (ddd, J = 7.5, 5.5, and 2.0 Hz, 1H), 3.89−3.86 (m, 1H), 3.74 (t, J = 10.0 Hz, 1H), and 3.57−3.51 (m, 2H). ^{19}F{^{1}H} NMR (470 MHz, D_2O): δ −231.2. ^{19}F NMR (470 MHz, D_2O): δ −231.2 (t, $^2J_{H1a,H1b,F}$ = 46.8 Hz). ^{31}P{^{1}H} NMR (202 MHz, D_2O): δ 4.1. ^{13}C{^{1}H} NMR (125 MHz, D_2O): δ 96.4 (d, $^2J_{C\text{-}2,F}$ = 21.3 Hz), 83.2 (d, $^1J_{C\text{-}1,F}$ = 174.4 Hz), 73.1, 72.2 (d, $^2J_{C\text{-}7,P}$ = 7.5 Hz), 70.4, 69.2, and 62.9 (d, $^3J_{C\text{-}6,P}$ = 4.0 Hz). HRMS (ESI$^-$): found $[M − H]^-$, 291.0274, $C_7H_{13}FO_9P$; requires $[M − H]^-$, 291.0287.

1-Deoxy-1,1-difluoro-α-D-gluco-heptulose 7-Phosphate (3). To a solution of freshly distilled diisopropylamine (0.80 mL, 5.74 mmol) in anhydrous THF (4.5 mL) at −78 °C was added dropwise *n*-BuLi (2.3 mL, 2.5 M in hexane, 5.74 mmol) under N_2. The solution was stirred for 30 min, allowed to warm to 0 °C, and stirred for an additional 30 min. The solution was then cooled to −78 °C. A solution of diethyldifluoromethylphosphonate (0.87 mL, 5.55 mmol) in anhydrous THF (1 mL) was added dropwise. The solution was stirred for 25 min and **5** (1.00 g, 1.85 mmol) in anhydrous THF (5 mL) was added dropwise. The solution was stirred for 30 min at −78 °C. When the reaction was complete, as determined by TLC monitoring, it was quenched by the addition of saturated aq NH$_4$Cl (3 mL) and diethyl ether (50 mL). The aqueous layer was further extracted with diethyl ether (3 × 15 mL). The combined organic layers were dried with anhydrous MgSO$_4$, filtered, and evaporated under reduced pressure. The residue obtained was used in the next step without further purification. An analytic amount of pure sample was obtained by silica gel flash chromatography (*n*-hexane/EtOAc = 4) for characterization purposes.

Data for 6 (Figures S19−S21). ^{1}H NMR (500 MHz, CDCl$_3$): δ 7.44−7.28 (m, 20H), 5.04−4.92 (m, 5H), 4.69 (d, J = 11.0 Hz, 1H), 4.63 (d, J = 11.9 Hz, 1H), 4.54 (d, J = 11.9

Hz, 1H), 4.46−4.33 (m, 4H), 4.26−4.23 (m, 1H), 4.20 (t, J = 9.3 Hz, 1H), 4.11−4.09 (m, 1H), 3.91 (dd, J = 11.1 and 3.9 Hz, 1H), 3.84 (t, J = 9.6 Hz, 1H), 3.78 (dd, J = 11.0 and 1.4 Hz, 1H), 1.46 (t, J = 7.1 Hz, 3H), and 1.38 (t, J = 7.1 Hz, 3H). ^{19}F NMR (470 MHz, CDCl$_3$): δ −119.5 (ABX, $^2J_{F,F}$ = 303.7 Hz, $^2J_{F,P}$ = 95.5 Hz), −120.3 (ABX, $^2J_{F,F}$ = 303.7 Hz, $^2J_{F,P}$ = 99.1 Hz). ^{31}P{^{1}H} NMR (202 MHz, CDCl$_3$): δ 6.6 (t, $^2J_{P,F}$ = 96.2 Hz). This data is consistent with those reported.[30]

Crude **6** and anhydrous K$_2$CO$_3$ (1.40 g, 10.18 mmol) were dissolved in anhydrous DMF (25 mL). The mixture was stirred at 55 °C under N_2. When the reaction was finished (about 3 h), as determined by TLC analysis, it was cooled to room temperature, H_2O (15 mL) was added, and the product was extracted with diethyl ether (4 × 50 mL). The combined organic extract was rinsed with H_2O (1 × 10 mL), dried using anhydrous MgSO$_4$, filtered, and evaporated under reduced pressure. The obtained residue was purified by silica gel flash chromatography with *n*-hexane/EtOAc (3:1 v/v) to give **7** (1.16 g, 86% over two steps) as a colorless oil.

Data for 7 (Figures S22−S25). ^{1}H NMR (500 MHz, CDCl$_3$): δ 7.44−7.28 (m, 20H), 6.57 (t, $^2J_{H\text{-}1,F}$ = 54 Hz, H-1), 4.97−4.89 (m, 5H), 4.73−4.71 (m, 2H), 4.63−4.61 (m, 1H), 4.24−4.16 (m, 5H), 4.09 (t, J = 9.4 Hz, 1H), 4.01 (dd, J = 9.4 and 4.0 Hz, 1H), 3.92 (dd, J = 11.5 and 3.6 Hz, 1H), 3.88 (t, J = 9.7 Hz, 1H), 3.81 (dd, J = 11.4 and 1.6 Hz, 1H), and 1.38−1.32 (m, 6H). ^{19}F{^{1}H} NMR (470 MHz, CDCl$_3$): δ −131.6 (d, $^2J_{F,F}$ = 285.9 Hz) and −133.7 (d, $^2J_{F,F}$ = 285.9 Hz). ^{19}F NMR (470 MHz, CDCl$_3$): δ −131.6 (d, $^2J_{F,F}$ = 285.9 Hz, $^2J_{H\text{-}1,F}$ = 53.7 Hz) and −133.7 (d, $^2J_{F,F}$ = 285.9 Hz, $^2J_{H\text{-}1,F}$ = 55.6 Hz). ^{31}P{^{1}H} NMR (202 MHz, CDCl$_3$): δ −5.85. ^{13}C{^{1}H} NMR (125 MHz, CDCl$_3$): δ 140.4, 140.2, 140.0, 139.9, 130.5, 130.4, 130.2, 130.0, 129.9, 129.87, 129.8, 129.7, 114.4 (t, $^1J_{C\text{-}1,F}$ = 248.5 Hz, C-1), 102.8 (dt, $^2J_{C\text{-}2,F}$ = 25.2 Hz, $^2J_{C\text{-}2,P}$ = 8.4 Hz, C-2), 84.4, 79.95 (d, J = 7.1 Hz), 79.4, 79.1, 79.0, 77.2, 75.5, 70.0, 66.4 (d, $^2J_{\text{−OCH}_2CH_3,P}$ = 5.8 Hz), 66.3 (d, $^2J_{\text{−OCH}_2CH_3,P}$ = 5.7 Hz), 18.1 (d, $^3J_{\text{−OCH}_2CH_3,P}$ = 6.8 Hz), and 18.0 (d, $^3J_{\text{−OCH}_2CH_3,P}$ = 6.8 Hz).

A solution of **7** (700 mg, 0.96 mmol) in 1,4-dioxane (3 mL) and 6 N HCl (3 mL) was refluxed at 100 °C overnight. The reaction was complete as determined by TLC monitoring. The solvent was evaporated in vacuo to give a residue which was dissolved in EtOAc (100 mL) and washed with saturated aq NaHCO$_3$ (15 mL). The organic layer was washed with H_2O (2 × 10 mL), then with brine (5 mL). The combined aqueous layer was further extracted with EtOAc (4 × 15 mL). The combined organic layer was dried over MgSO$_4$, filtered, and evaporated under reduced pressure. The residue obtained was purified by silica gel flash chromatography with *n*-hexane/EtOAc (6:1 v/v) to give **8** (307 mg, 54% yield) as a light yellow oil.

Data for 8 (Figures S26 and S27). ^{1}H NMR (500 MHz, CDCl$_3$): δ 7.34−7.14 (m, 20H), 5.61 (t, $^2J_{H\text{-}1,F}$ = 55 Hz, 1H), 4.87−4.50 (m, 8H), 4.00 (m, 1H), 3.93 (m, 1H), 3.84−3.77 (m, 2H), 3.75−3.66 (m, 2H), and 3.52 (s, br, 1H, OH). ^{19}F{^{1}H} NMR (470 MHz, CDCl$_3$): δ −133.4 (d, $^2J_{Fa,Fb}$ = 283 Hz) and −136.4 (d, $^2J_{Fa,Fb}$ = 283 Hz). ^{19}F NMR (470 MHz, CDCl$_3$): δ −133.4 (dd, $^2J_{Fa,Fb}$ = 283 Hz, $^2J_{Fa,H\text{-}1}$ = 55 Hz) and −136.4 (dd, $^2J_{Fb,Fa}$ = 283 Hz, $^2J_{Fb,H\text{-}1}$ = 56 Hz). These data are consistent with those reported.[31]

To a solution of **8** (50 mg, 0.085 mmol) in CH_3OH was added 20% wt Pd(OH)$_2$/C (10 mg). The suspension was

degassed under vacuum and saturated with H_2 in a 1 atm balloon. The reaction mixture was stirred overnight. When the starting material was consumed, as determined by TLC analysis, the catalyst was filtered off. The filtrate was concentrated under reduced pressure to give **14** (19 mg, 100%).

Data for 14 (Figures S28–S30). ^1H NMR (500 MHz, D_2O): δ 5.94 (t, $^2J_{H-1,F}$ = 54 Hz, 1H, H-1), 3.93−3.70 (m, 4H), 3.68 (d, J = 10 Hz, 1H), and 3.51 (t, J = 9 Hz, 1H). $^{19}F\{^1H\}$ NMR (282 MHz, D_2O): δ −133.2 (d, $^2J_{Fa−Fb}$ = 286 Hz) and −140.7 ($^2J_{Fa−Fb}$ = 286 Hz). ^{19}F NMR (282 MHz, D_2O): δ −133.2 (dd, $^2J_{Fa,Fb}$ = 286 Hz, $^2J_{Fa,H}$ = 54 Hz, 1F) and −140.7 (dd, $^2J_{Fb,Fa}$ = 286 Hz, $^2J_{Fb,H}$ = 54 Hz, 1F). $^{13}C\{^1H\}$ NMR (125 MHz, D_2O): δ 133.3 (t, $^1J_{C-1,F}$ = 249 Hz, C-1), 94.6 (t, $^2J_{C-2,F}$ = 94.6 Hz, C-2), 73.4, 72.8, 70.2, 69.2, and 60.4. HRMS (ESI/TOF) m/z: $[M + Na]^+$ calcd for $C_7H_{12}O_6F_2Na$, 253.0494; found, 253.0493.

Following the general procedure, **3** (17 mg, 92% yield) was obtained from compound **14** (13.8 mg, 60 μM), $MgCl_2$ (122 mg, 600 μM), ATP (200 mM, 600 μL), Glk (28 mg mL^{-1}, 110 μL), and Tris−HCl (50 mM, 3290 μL, pH 7.5).

Data for 3 (Figures S31–S34). ^1H NMR (500 MHz, D_2O): δ 5.86 (t, $^2J_{H1,F}$ = 55.0 Hz, 1H), 4.05−4.00 (m, 1H), 3.98−3.95 (m, 1H), 3.89−3.87 (m, 1H), 3.74−3.69 (m, 1H), 3.62−3.60 (m, 1H), and 3.52 (t, J = 10.0 Hz, 1H). $^{19}F\{^1H\}$ NMR (470 MHz, D_2O): δ −133.3 (d, $^2J_{F,F}$ = 286.7 Hz) and −141.1 (d, $^2J_{F,F}$ = 286.7 Hz). ^{19}F NMR (470 MHz, D_2O): δ −133.3 (dd, $^2J_{H,F}$ = 54.4 Hz, $^2J_{F,F}$ = 286.7 Hz) and −141.1 (dd, $^2J_{H,F}$ = 54.4 Hz, $^2J_{F,F}$ = 286.7 Hz). $^{31}P\{^1H\}$ NMR (202 MHz, D_2O): δ 3.1. $^{13}C\{^1H\}$ NMR (125 MHz, D_2O): δ 113.2 (t, $^1J_{C-1,F}$ = 247.5 Hz, C-1), 94.8 (t, $^2J_{C-2,F}$ = 21.3 Hz, C-2), 73.1, 72.3 (d, $^2J_{C-7,P}$ = 7.5 Hz, C-7), 70.3, 68.8, and 62.9 (d, $^3J_{C-6,P}$ = 3.9 Hz, C-6), HRMS (ESI$^-$): found $[M − H]^-$, 309.0181, $C_7H_{12}F_2O_9P$; requires $[M − H]^-$, 309.0192.

1-Deoxy-1-trifluoro-α-D-gluco-heptulose 7-Phosphate (4). Compound **11** was prepared by treatment of lactone **5** with $TMSCF_3$ in THF, according to a literature method.[28] Data for **11** (Figure S35): ^{19}F NMR (470 MHz, D_2O): δ −83.4. This data is consistent with that reported.[28]

To a solution of **11** (110 mg, 0.181 mmol) in CH_3OH, Pd/C (20 mg) was added. The suspension was degassed under vacuum and saturated with H_2 in a Parr shaker at 60 psi pressure. This reaction mixture was shaken for 3 days until the starting material disappeared, as determined by TLC analysis. The catalyst was filtered off, and the filtrate was concentrated under reduced pressure to give **15** (44.4 mg, 100%).

Data for 15 (Figures S36–S38). ^1H NMR (500 MHz, D_2O): δ 3.76−3.67 (m, 3H), 3.63−3.62 (m, 2H), and 3.41−3.38 (m, 1H). $^{19}F\{^1H\}$ NMR (470 MHz, D_2O): δ −82.5 (s). ^{19}F NMR (470 MHz, D_2O): δ −82.5 (s). $^{13}C\{^1H\}$ NMR (125 MHz, D_2O): δ 122.3 (q, $^1J_{C-1,F}$ = 285.6 Hz, C-1), 94.5 (q, $^2J_{C-2,F}$ = 30.1 Hz, C-2), 73.3, 73.0, 70.0, 68.7, and 60.0, HRMS (ESI$^+$): found $[M + Na]^+$, 271.0406, $C_7H_{11}F_3NaO_6$; requires $[M + Na]^+$, 271.0400.

Following the general procedure, **4** (15.7 mg, 98%) was obtained from compound **15** (12.5 mg, 50 μM), $MgCl_2$ (102 mg, 500 μM), ATP (200 mM, 500 μL), Glk (28 mg mL^{-1}, 110 μL), and Tris−HCl (50 mM, 3390 μL, pH 7.5).

Data for 4 (Figures S39–S42). ^1H NMR (500 MHz, D_2O): δ 4.034 (ddd, J = 12.0, 7.5 and 4.5 Hz, 1H), 3.98 (ddd, J = 7.6, 5.7 and 1.9 Hz, 1H), 3.89−3.86 (m, 1H), 3.73−3.68 (m, 2H), and 3.59−3.55 (m, 1H). $^{19}F\{^1H\}$ NMR (470 MHz, D_2O): δ

−82.4. ^{19}F NMR (470 MHz, D_2O): δ −82.4. $^{31}P\{^1H\}$ NMR (202 MHz, D_2O): δ 2.8. $^{13}C\{^1H\}$ NMR (125 MHz, D_2O): δ 122.4 (q, $^1J_{C-1,F}$ = 286.3 Hz, C-1), 94.8 (q, $^2J_{C-2,F}$ = 31.3 Hz, C-1), 73.1, 72.6 (d, $^2J_{C-7,P}$ = 7.5 Hz, C-7), 70.2, 68.6, and 62.9 (d, $^3J_{C-7,P}$ = 4.0 Hz, C-6). HRMS (ESI$^-$): found $[M − H]^-$, 327.0103, $C_7H_{11}F_3O_9P$; requires $[M − H]^-$, 327.0098.

Protein Overexpression and Purification. βPGM, αPMM/PGM, and Glk were overexpressed, purified, and quantified as previously described.[40] The gene for XcPGM was commercially synthesized (GenScript) and inserted into the pET-14B vector with an N-terminal tobacco etch virus (TEV) protease cleavage site and His$_6$-affinity tag. The plasmid was transformed into *E. coli* BL31(DE3) for recombinant protein expression. Cultures were grown at 37 °C in LB media, supplemented with 0.1 mg mL^{-1} of ampicillin to an OD_{600} of 0.8−1.0. Cultures were then cooled at 4 °C for at least 30 min, whereby, isopropyl 1-thio-β-D-galactopyranoside (final concentration 0.4 mM) was added, and the cultures were incubated for ~18 h at 18 °C. Cell pellets were collected by centrifugation, flash frozen in liquid N_2, and stored at −80 °C.

For purification, frozen cell pellets were resuspended in buffer A (20 mM sodium phosphate, 0.3 M NaCl, pH 7.8) containing 14.4 mM β-mercaptoethanol, 0.5 mM phenylmethylsulfonyl fluoride (PMSF), 0.5 mM tosyllysine chloromethyl ketone, 2 mM $CaCl_2$, 2 mM $MgSO_4$, and 10 $\mu g/mL$ of DNase. A French press was used for cell lysis. The soluble fraction containing XcPGM was obtained through centrifugation. Protamine sulfate was added at 5 mg/g of cell pellet over 15 min, stirred for 30 min, and centrifuged. The supernatant was mixed with Ni^{2+} affinity resin (His-Select, Sigma), which had been previously equilibrated in buffer A, and incubated for 30 min on a two-way orbital rocker. The mixture was transferred into a gravity-packed column and washed with buffer A containing 5 mM imidazole, pH 7.8. Protein was eluted using buffer A supplemented with 250 mM imidazole, pH 7.8. The purified protein was dialyzed into a solution of 50 mM Tris HCl, pH 8.0, with 0.3 M NaCl. TEV protease was added to the purified protein at 5% w/w. The mixture was incubated at room temperature for 4 h and left overnight at 4 °C. The mixture was then incubated with pre-equilibrated Ni^{2+} affinity resin for 30 min. Cleaved XcPGM was retrieved in the flow-through and dialyzed into 20 mM Tris HCl, pH 7.4, with 0.3 M NaCl and concentrated to ~11 mg mL^{-1}. The purified protein was flash-frozen in liquid nitrogen and stored at −80 °C. Total yield of protein from 1 L of cell culture was ~80 mg.

Crystallization and Complex Formation. Purified XcPGM was initially screened for crystallization via hanging-drop vapor diffusion using the previously published conditions,[37] which did not yield data collection quality crystals. Several commercial screens were then utilized, including Morpheus 1 and Hampton Crystal Screen 1. Optimizations were set up around several hits, and a final condition of 22% PEG 8000, 0.2 M $MgCl_2$, 0.1 M HEPES, pH 7.5, was identified and used for all crystals described herein. Crystals typically grew overnight at 18 °C. Despite the different crystallization conditions, the XcPGM crystals reported here were isomorphous with those published previously (Table S2).

The CH3G6P complex was obtained by soaking crystals with high concentrations of the ligand. The ligand solution at ~20 mM was prepared in the crystallization buffer supplemented with cryoprotectant of 25−30% PEG 3350. Crystals were removed from the drop, dipped quickly into the

ligand solution, and immediately flash-cooled and stored in liquid N$_2$.

X-ray Diffraction Data Collection and Refinement. Diffraction data were collected at a wavelength of 1.00003 Å from single crystals on beamline 4.2.2 of the advanced light source using a Taurus-1 CMOS detector in the shutterless mode. Data were processed using XDS[41] and AIMLESS[42] in CCP4i.[43] Data processing statistics are listed in Table S1 (see the Supporting Information). Values of CC$_{1/2}$ > 0.30[44] and R_{pim}[45] were used to determine the high resolution cutoff due to the large number of images (900−3600 per data set) and high redundancy obtained with the shutterless data collection.

Crystallographic refinement calculations were initiated using coordinates of apo-XcPGM (PDB ID: 5BMN). Refinement was performed with PHENIX;[46] progress was monitored by following R_{free}, with 5% of each data-set set aside for cross validation. The B-factor model consisted of an isotropic B-factor for each atom; TLS refinement was used as automated in PHENIX. Occupancy of the ligand was also refined and converged at 0.82. COOT[47] was used for model building. The structures were validated using MolProbity,[48] and the refinement statistics are listed in Table S1 (see the Supporting Information). Likely hydrogen bond criteria and lengths were determined by CONTACT in CCP4.[43] Structural figures were prepared with PYMOL.[49] The coordinates and structure factor amplitudes have been deposited in the PDB under the accession numbers listed in Table S1 (see the Supporting Information).

Kinetic Inhibition Assays (IC$_{50}$ Determination) of Analogues 1−4 Against αPMM/PGM and βPGM. *IC$_{50}$ Determination of βPGM.* Assays were carried out in a final volume of 200 μL containing 50 mM HEPES pH 7.2, 2 mM MgCl$_2$, 0.5 mM NAD$^+$, 5 U/mL G6PDH, 150 μM αF16BP, 10 μM βG1P, 83 nM βPGM, and 5−1000 μM inhibitor (1−4). βPGM was pre-incubated with αF16BP for 30−45 min. Reactions were initiated by addition of the pre-incubated βPGM/F16BP mixture to the remaining reaction components.

IC$_{50}$ Determination of αPMM/PGM. Assays were conducted in a final volume of 200 μL containing 50 mM MOPS buffer pH 7.4, 3.6 mM MgCl$_2$, 0.9 mM NAD$^+$, 1 mM EDTA, 1 mM DTT, 5 U/mL G6PDH, 2 μM αG16P, 20 μM αG1P, 0.242 μM αPGM/PMM, and 5−1000 μM inhibitor (1−4). αPMM/PGM was pre-incubated with αG16P for 1−1.5 h. Reactions were initiated by addition of the pre-incubated αPMM/PGM/αG16P mixture to the remaining reaction components.

■ ASSOCIATED CONTENT

ⓈSupporting Information

The Supporting Information is available free of charge on the ACS Publications website at DOI: 10.1021/acsomega.9b00008.

> ^{19}F{^{1}H} NMR and ^{31}P{^{1}H} NMR spectra comparison of phosphonate 6 and phosphate 7, the activity (plots) of αPMM/PGM and βPGM in response to inhibitors (1−4), sequence alignment of *X. citri* PGM and *P. aeruginosa* PMM/PGM, X-ray data collection and refinement statistics for 1 complex, polder omit map, characterization data, and NMR spectra of new compounds (1−4, 7, 12, 14 and 15) (PDF)

■ AUTHOR INFORMATION

Corresponding Authors
*E-mail: beamerl@missouri.edu (L.J.B.).
*E-mail: David.Jakeman@dal.ca (D.L.J.).

ORCID ◉
Lesa J. Beamer: 0000-0001-5689-200X
David L. Jakeman: 0000-0003-3002-3388

Author Contributions
¶S.M.W., A.D.G., and A.F.V. contributed equally.

Notes
The authors declare no competing financial interest.

■ REFERENCES

(1) Jacobsen, A.; Thiem, J. Contemporary Syntheses of 2-Ketoheptoses and Derivatives. *Curr. Org. Chem.* **2014**, *18*, 2833−2841.

(2) (a) Blomberg, B. A.; Codreanu, I.; Cheng, G.; Werner, T. J.; Alavi, A. Beta-Cell Imaging: Call for Evidence-Based and Scientific Approach. *Mol. Imaging Biol.* **2013**, *15*, 123−130. (b) Tiedge, M. Inside the pancreas: progress and challenges of human beta cell mass quantification. *Diabetologia* **2014**, *57*, 856−859. (c) Jodal, A.; Schibli, R.; Béhé, M. Targets and probes for non-invasive imaging of β-cells. *Eur. J. Nucl. Med. Mol. Imaging* **2017**, *44*, 712−727.

(3) Malaisse, W. J.; Zhang, Y.; Louchami, K.; Sharma, S.; Dresselaers, T.; Himmelreich, U.; Novotny, G. W.; Mandrup-Poulsen, T.; Waschke, D.; Leshch, Y.; Thimm, J.; Thiem, J.; Sener, A. 19F-heptuloses as tools for the non-invasive imaging of GLUT2-expressing cells. *Arch. Biochem. Biophys.* **2012**, *517*, 138−143.

(4) Chen, Y.; Wang, X.; Wang, J.; Yang, Y. Synthesis of D-manno-heptulose via a cascade aldol/hemiketalization reaction. *Beilstein J. Org. Chem.* **2017**, *13*, 795−799.

(5) (a) Subrizi, F.; Cárdenas-Fernández, M.; Lye, G. J.; Ward, J. M.; Dalby, P. A.; Sheppard, T. D.; Hailes, H. C. Transketolase catalysed upgrading of l-arabinose: the one-step stereoselective synthesis of l-gluco-heptulose. *Green Chem.* **2016**, *18*, 3158−3165. (b) Yang, J.; Zhu, Y.; Li, J.; Men, Y.; Sun, Y.; Ma, Y. Biosynthesis of rare ketoses through constructing a recombination pathway in an engineeredCorynebacterium glutamicum. *Biotechnol. Bioeng.* **2015**, *112*, 168−180.

(6) Kim, J.-H.; Resende, R.; Wennekes, T.; Chen, H.-M.; Bance, N.; Buchini, S.; Watts, A. G.; Pilling, P.; Streltsov, V. A.; Petric, M.; Liggins, R.; Barrett, S.; McKimm-Breschkin, J. L.; Niikura, M.; Withers, S. G. Mechanism-Based Covalent Neuraminidase Inhibitors with Broad-Spectrum Influenza Antiviral Activity. *Science* **2013**, *340*, 71−75.

(7) Onega, M.; Winkler, M.; O'Hagan, D. Fluorinase: a tool for the synthesis of 18F-labeled sugars and nucleosides for PET. *Future Med. Chem.* **2009**, *1*, 865−873.

(8) Matei, E.; André, S.; Glinschert, A.; Infantino, A. S.; Oscarson, S.; Gabius, H.-J.; Gronenborn, A. M. Fluorinated Carbohydrates as Lectin Ligands: Dissecting Glycan−Cyanovirin Interactions by Using 19F NMR Spectroscopy. *Chem.—Eur. J.* **2013**, *19*, 5364−5374.

(9) Linclau, B.; Wang, Z.; Compain, G.; Paumelle, V.; Fontenelle, C. Q.; Wells, N.; Weymouth-Wilson, A. Investigating the Influence of (Deoxy)fluorination on the Lipophilicity of Non-UV-Active Fluorinated Alkanols and Carbohydrates by a New log P Determination Method. *Angew. Chem., Int. Ed.* **2016**, *55*, 674−678.

(10) Whitehouse, D. B.; Tomkins, J.; Lovegrove, J. U.; Hopkinson, D. A.; McMillan, W. O. A phylogenetic approach to the identification of phosphoglucomutase genes. *Mol. Biol. Evol.* **1998**, *15*, 456−462.

(11) Lahiri, S. D.; Zhang, G.; Dunaway-Mariano, D.; Allen, K. N. Caught in the Act: The Structure of Phosphorylated β-Phosphoglucomutase from Lactococcus lactis. *Biochemistry* **2002**, *41*, 8351−8359.

(12) Levander, F.; Andersson, U.; Radstrom, P. Physiological Role of β-Phosphoglucomutase inLactococcus lactis. *Appl. Environ. Microbiol.* **2001**, *67*, 4546−4553.

(13) Stiers, K. M.; Muenks, A. G.; Beamer, L. J. Biology, Mechanism, and Structure of Enzymes in the α-d-Phosphohexomutase Superfamily. *Advances in Protein Chemistry and Structural Biology*; Academic Press, 2017; Vol. 109, pp 265−304.

(14) Regni, C.; Tipton, P. A.; Beamer, L. J. Crystal Structure of PMM/PGM. *Structure* **2002**, *10*, 269−279.

(15) Willyard, C. The drug-resistant bacteria that pose the greatest health threats. *Nature* **2017**, *543*, 15.

(16) Huang, Y. L.; Ebner, K. E. Inhibition of phosphoglucomutase by galactose 1,6-diphosphate. *Experientia* **1969**, *25*, 917−918.

(17) Galloway, C. M.; Dugger, W. M.; Black, C. C. Fructose 2,6-Bisphosphate Inhibition of Phosphoglucomutase. *Plant Physiol.* **1988**, *88*, 980−982.

(18) Naught, L. E.; Tipton, P. A. Kinetic Mechanism and pH Dependence of the Kinetic Parameters of Pseudomonas aeruginosa Phosphomannomutase/Phosphoglucomutase. *Arch. Biochem. Biophys.* **2001**, *396*, 111−118.

(19) Percival, M. D.; Withers, S. G. Synthesis and testing of sugar phosphofluoridates and cyclic phosphates as inhibitors of phosphoglucomutase. *J. Org. Chem.* **1992**, *57*, 811−817.

(20) Kim, S. C.; Raushel, F. M. Mechanism-based inactivation of rabbit muscle phosphoglucomutase by nojirimycin 6-phosphate. *Biochemistry* **1988**, *27*, 7328−7332.

(21) Percival, M. D.; Doherty, K.; Gresser, M. J. Inhibition of phosphoglucomutase by vanadate. *Biochemistry* **1990**, *29*, 2764−2769.

(22) Jin, Y.; Richards, N. G.; Waltho, J. P.; Blackburn, G. M. Metal Fluorides as Analogues for Studies on Phosphoryl Transfer Enzymes. *Angew. Chem., Int. Ed.* **2017**, *56*, 4110−4128.

(23) (a) Baxter, N. J.; Bowler, M. W.; Alizadeh, T.; Cliff, M. J.; Hounslow, A. M.; Wu, B.; Berkowitz, D. B.; Williams, N. H.; Blackburn, G. M.; Waltho, J. P. Atomic details of near-transition state conformers for enzyme phosphoryl transfer revealed by Formula rather than by phosphoranes. *Proc. Natl. Acad. Sci. U.S.A.* **2010**, *107*, 4555−4560. (b) Griffin, J. L.; Bowler, M. W.; Baxter, N. J.; Leigh, K. N.; Dannatt, H. R. W.; Hounslow, A. M.; Blackburn, G. M.; Webster, C. E.; Cliff, M. J.; Waltho, J. P. Near attack conformers dominate -phosphoglucomutase complexes where geometry and charge distribution reflect those of substrate. *Proc. Natl. Acad. Sci. U.S.A.* **2012**, *109*, 6910−6915.

(24) (a) Jin, Y.; Bhattasali, D.; Pellegrini, E.; Forget, S. M.; Baxter, N. J.; Cliff, M. J.; Bowler, M. W.; Jakeman, D. L.; Blackburn, G. M.; Waltho, J. P. α-Fluorophosphonates reveal how a phosphomutase conserves transition state conformation over hexose recognition in its two-step reaction. *Proc. Natl. Acad. Sci. U.S.A.* **2014**, *111*, 12384−12389. (b) Ampaw, A.; Carroll, M.; von Velsen, J.; Bhattasali, D.; Cohen, A.; Bowler, M. W.; Jakeman, D. L. Observing enzyme ternary transition state analogue complexes by 19F NMR spectroscopy. *Chem. Sci.* **2017**, *8*, 8427−8434.

(25) Meyer, D.; Schneider-Fresenius, C.; Horlacher, R.; Peist, R.; Boos, W. Molecular characterization of glucokinase from Escherichia coli K-12. *J. Bacteriol.* **1997**, *179*, 1298−1306.

(26) Lay, L.; Nicotra, F.; Panza, L.; Russo, G.; Caneva, E. Synthesis of C-disaccharides through dimerization of exo-glycals. *J. Org. Chem.* **1992**, *57*, 1304−1306.

(27) Leshch, Y.; Waschke, D.; Thimm, J.; Thiem, J. d-Gluco-hept-2-ulose and Novel Deoxyfluoro Derivatives as Seven-Carbon Analogues of F-Deoxy-d-glucose (FDG). *Synthesis* **2011**, 3871−3877.

(28) Magueur, G.; Crousse, B.; Ourévitch, M.; Bonnet-Delpon, D.; Bégué, J.-P. Fluoro-artemisinins: When a gem-difluoroethylene replaces a carbonyl group. *J. Fluorine Chem.* **2006**, *127*, 637−642.

(29) (a) Beier, P.; Alexandrova, A. V.; Zibinsky, M.; Surya Prakash, G. K. Nucleophilic difluoromethylation and difluoromethylenation of aldehydes and ketones using diethyl difluoromethylphosphonate.

Tetrahedron **2008**, *64*, 10977−10985. (b) Beier, P.; Pohl, R.; Alexandrova, A. An Efficient and Highly Selective Synthesis of (Z)-Fluoroenol Phosphates from Hydroxy Difluorophosphonates. *Synthesis* **2009**, 957−962.

(30) Forget, S. M.; Bhattasali, D.; Hart, V. C.; Cameron, T. S.; Syvitski, R. T.; Jakeman, D. L. Synthesis and enzymatic evaluation of ketose phosphonates: the interplay between mutarotation, monofluorination and acidity. *Chem. Sci.* **2012**, *3*, 1866−1878.

(31) Liu, X.; Yin, Q.; Yin, J.; Chen, G.; Wang, X.; You, Q.-D.; Chen, Y.-L.; Xiong, B.; Shen, J. Highly Stereoselective Nucleophilic Addition of Difluoromethyl-2-pyridyl Sulfone to Sugar Lactones and Efficient Synthesis of Fluorinated 2-Ketoses. *Eur. J. Org. Chem.* **2014**, 6150−6154.

(32) Kwan, D. H.; Jin, Y.; Jiang, J.; Chen, H.-M.; Kötzler, M. P.; Overkleeft, H. S.; Davies, G. J.; Withers, S. G. Chemoenzymatic synthesis of 6-phospho-cyclophellitol as a novel probe of 6-phospho-β-glucosidases. *FEBS Lett.* **2016**, *590*, 461−468.

(33) (a) Zhang, G.; Dai, J.; Wang, L.; Dunaway-Mariano, D.; Tremblay, L. W.; Allen, K. N. Catalytic Cycling in β-Phosphoglucomutase: A Kinetic and Structural Analysis. *Biochemistry* **2005**, *44*, 9404−9416. (b) Schramm, A. M.; Mehra-Chaudhary, R.; Furdui, C. M.; Beamer, L. J. Backbone Flexibility, Conformational Change, and Catalysis in a Phosphohexomutase fromPseudomonas aeruginosa. *Biochemistry* **2008**, *47*, 9154−9162.

(34) Cer, R. Z.; Mudunuri, U.; Stephens, R.; Lebeda, F. J. IC50-to-Ki: a web-based tool for converting IC50 to Ki values for inhibitors of enzyme activity and ligand binding. *Nucleic Acids Res.* **2009**, *37*, W441−W445.

(35) (a) Meanwell, N. A. Fluorine and fluorinated motifs in the design and application of bioisosteres for drug design. *J. Med. Chem.* **2018**, *61*, 5822−5880. (b) Kitazume, T.; Yamazaki, T. *Experimental methods in organic fluorine chemistry*. CRC Press, 1999; Vol. 9.

(36) Huheey, J. E. The Electronegativity of Groups. *J. Phys. Chem.* **1965**, *69*, 3284−3291.

(37) Goto, L. S.; Vessoni Alexandrino, A.; Malvessi Pereira, C.; Silva Martins, C.; D'Muniz Pereira, H.; Brandão-Neto, J.; Marques Novo-Mansur, M. T. Structural and functional characterization of the phosphoglucomutase from Xanthomonas citri subsp. citri. *Biochim. Biophys. Acta, Proteins Proteomics* **2016**, *1864*, 1658−1666.

(38) Regni, C.; Naught, L.; Tipton, P. A.; Beamer, L. J. Structural basis of diverse substrate recognition by the enzyme PMM/PGM from P. aeruginosa. *Structure* **2004**, *12*, 55−63.

(39) Li, X.; Ohtake, H.; Takahashi, H.; Ikegami, S. A facile synthesis of 1′-C-alkyl-α-disaccharides from 1-C-alkyl-hexopyranoses and methyl 1-C-methyl-hexopyranosides. *Tetrahedron* **2001**, *57*, 4297−4309.

(40) Timmons, S. C.; Mosher, R. H.; Knowles, S. A.; Jakeman, D. L. Exploiting Nucleotidylyltransferases To Prepare Sugar Nucleotides. *Org. Lett.* **2007**, *9*, 857−860.

(41) Kabsch, W. Xds. *Acta Crystallogr., Sect. D: Biol. Crystallogr.* **2010**, *66*, 125−132.

(42) Evans, P. R.; Murshudov, G. N. How good are my data and what is the resolution? *Acta Crystallogr., Sect. D: Biol. Crystallogr.* **2013**, *69*, 1204−1214.

(43) Potterton, E.; Briggs, P.; Turkenburg, M.; Dodson, E. A graphical user interface to the CCP4 program suite. *Acta Crystallogr., Sect. D: Biol. Crystallogr.* **2003**, *59*, 1131−1137.

(44) Karplus, P. A.; Diederichs, K. Linking crystallographic model and data quality. *Science* **2012**, *336*, 1030−1033.

(45) Weiss, M. S. Global indicators of X-ray data quality. *J. Appl. Crystallogr.* **2001**, *34*, 130−135.

(46) Adams, P. D.; Afonine, P. V.; Bunkóczi, G.; Chen, V. B.; Davis, I. W.; Echols, N.; Headd, J. J.; Hung, L.-W.; Kapral, G. J.; Grosse-Kunstleve, R. W.; McCoy, A. J.; Moriarty, N. W.; Oeffner, R.; Read, R. J.; Richardson, D. C.; Richardson, J. S.; Terwilliger, T. C.; Zwart, P. H. PHENIX: a comprehensive Python-based system for macromolecular structure solution. *Acta Crystallogr., Sect. D: Biol. Crystallogr.* **2010**, *66*, 213−221.

(47) Emsley, P.; Cowtan, K. Coot: model-building tools for molecular graphics. *Acta Crystallogr., Sect. D: Biol. Crystallogr.* **2004**, *60*, 2126−2132.

(48) Chen, V. B.; Arendall, W. B.; Headd, J. J.; Keedy, D. A.; Immormino, R. M.; Kapral, G. J.; Murray, L. W.; Richardson, J. S.; Richardson, D. C. MolProbity: all-atom structure validation for macromolecular crystallography. *Acta Crystallogr., Sect. D: Biol. Crystallogr.* **2010**, *66*, 12−21.

(49) Stierand, K.; Rarey, M. Drawing the PDB: Protein−Ligand Complexes in Two Dimensions. *ACS Med. Chem. Lett.* **2010**, *1*, 540−545.